

# Isotropy Test with Quasars Using Method of Smoothed Residuals

A. Antony,<sup><sup>a,b</sup></sup>

S. A. Appleby,<sup><sup>a,b</sup></sup>

W. L. Matthewson<sup><sup>c</sup></sup>

A.

Shafieloo<sup><sup>c</sup></sup>

<sup>a</sup>Asia Pacific Center for Theoretical Physics, Pohang, 37673, Republic of Korea

<sup>b</sup>Department of Physics, POSTECH, Pohang, 37673, Republic of Korea

<sup>c</sup>Korea Astronomy and Space Science Institute, 776, Daedeokdae-ro, Yuseong-gu, Daejeon 34055, Republic of Korea

E-mail: [akhilantony91@gmail.com](mailto:akhilantony91@gmail.com), [stephen.appleby@apctp.org](mailto:stephen.appleby@apctp.org)

**Abstract.** To assess the significance and scale dependence of anomalous large scale modes in the CatWISE quasar data, we generate smoothed number density fields on the sphere and study their extreme values – maximum, minimum, maximum antipodal difference. By comparing these summary statistics to those obtained from random isotropic realisations of the data, we determine the statistical significance of large scale modes as a function of smoothing scale. We perform our analysis using five different versions of the data – the original quasar map, the maps after separately subtracting the ecliptic bias and the CMB dipole, the map obtained after subtracting both, and the map after subtracting the ecliptic bias and anomalous dipole inferred in [1]. We find that the ecliptic-corrected, CMB dipole-removed map exhibits large scale modes that are in tension with random realisations of the data (p-values  $p \sim 10^{-4}$ ), over a wide range of smoothing scales  $\pi/8 \leq \delta \leq \pi/2$ . The most prominent feature in the data is an underdensity in the southern galactic plane at  $(b, \ell) = (-31^\circ, 78^\circ)$ , which reaches its highest statistical significance when smoothed on scales  $\delta = \pi/6$  ( $p \ll 10^{-5}$ ). Notably, the minima statistics align with the maximum antipodal difference statistics, whereas the maxima do not. This suggests that the observed dipole-like behavior in the data is primarily driven by the underdensity in the southern sky. The ecliptic corrected, anomalous dipole subtracted map reduces the significance of any residual anisotropic features, but an underdensity in the south sky persists with p-value  $p = 0.0018$ .

---

## Contents

<b>1</b>	<b>Introduction</b>	<b>1</b>
<b>2</b>	<b>Data</b>	<b>2</b>
<b>3</b>	<b>Methodology</b>	<b>3</b>
<b>4</b>	<b>Results</b>	<b>5</b>
4.1	Full Data Density Map	6
4.2	Full Data Density Map After Removing the CMB Dipole Signal	7
4.3	Ecliptic-Corrected Density Map	7
4.4	Ecliptic-Corrected & CMB Dipole Removed Density Map	11
4.5	Ecliptic-Corrected & Anomalous Dipole Removed Density Map	13
<b>5</b>	<b>Discussion</b>	<b>15</b>
<b>A</b>	<b>Appendix</b>	<b>16</b>
A.1	Removing a dipole signal from a radio source map	16

---

## 1 Introduction

Testing the foundational aspects of the standard cosmological model remains a challenging yet essential endeavor in modern cosmology. Within the FLRW description of our Universe, large scale statistical isotropy (SI) and homogeneity are imposed, which allows us to define spatially averaged energy densities that in turn source an average (monopole) expansion rate. On this background, perturbation theory is applied; the ensemble average of density fluctuations are also taken to be rotationally and translationally invariant. These assumptions are difficult to test; inferring the existence of an anisotropic signal requires directionally-sensitive summary statistics [2, 3], and there are many subtleties associated with tests of homogeneity [4–7]. Despite these difficulties, extensive efforts have been made to probe these fundamental symmetries. A range of studies, spanning cosmic microwave background analyses, large-scale structure surveys, and other cosmological observations, have sought to identify possible departures from isotropy and homogeneity [1, 8–26]. The results of these investigations continue to refine our understanding of the large-scale structure of the Universe and test the fundamental assumptions underpinning modern cosmology.

We can expect some degree of violation of isotropy as a function of scale, even within the standard model. In particular, on small scales, isotropy will be violated by the peculiar motion of objects with respect to the cosmic rest frame<sup>1</sup>. The precise consistency between the local bulk motion and the standard model is an open question and requires further study with deeper catalogs [12, 27, 28]. However, isotropy on the largest scales can be tested using certain data because it predicts that the last scattering surface as measured by CMB photons, and also any magnitude-limited sample of distant large scale structure tracer particles, should present a spherical distribution with respect to our observer location, after accounting for all relevant peculiar velocities. The presence of a large dipole in the CMB photon distribution is

---

<sup>1</sup>Assuming that such a rest frame exists.

attributed to our peculiar motion with respect to the last scattering surface<sup>2</sup>, and because the matter distribution in the high redshift Universe should be at rest with respect to the CMB, the application of the same velocity correction to the observed matter field should render it statistically isotropic. Using this idea, recent precision tests of the distribution of quasars on the sky have challenged the existence of a cosmological rest frame. Both CatWISE quasars [31] and NVSS radio galaxy data [32] present an excess dipole in number counts [1, 33], with an amplitude that is several times larger than the dipole measured from the CMB. Historically both excess dipoles [11, 14, 20, 21, 34–36] and a dipole consistent with the CMB [13, 37–42] have been found in large scale structure catalogs, but never with the statistical significance of recent work [1]. The result was subsequently confirmed in a number of works [42–44], but was also challenged in [26, 40]. The latter argued that additional large-scale features are present in the data and that the sky mask, which covers approximately 50% of the sky, can introduce mode coupling effects that influence the recovered multipoles and their statistical significance.

Given how central the assumption of isotropy is to building the standard model, testing it using a variety of methodologies is a rational approach. In this work, we apply a different set of statistics to the CatWISE data, with the goal of exploring the statistical significance of the large scale features. Specifically, we generate density fields by smoothing the quasar point distribution on the sky and examine particular one-point and restricted two-point summary statistics, which are the extreme values (maximum, minimum) of the field. One-point statistics provide complementary information compared to higher points, and are less affected by the presence of a mask. Conversely, there is generically less information in the one point statistics of a field compared to two-point measures (like a pair count). By measuring the extreme field values as we vary the smoothing length, we can build an understanding of the typical scales that are anomalous within the data and the extent to which they are anomalous.

The paper will proceed as follows. In Sections 2, 3 we review the data that will be analysed, and the statistics extracted from the quasars, respectively. We present our results in Section 4 and conclude with a discussion in Section 5.

## 2 Data

For the purpose of our study, we utilize an all-sky flux-limited quasar sample generated from the Wide-field Infrared Survey Explorer (WISE) mission [10]. WISE surveyed the sky in four infrared bands  $W1(3.4\mu\text{m})$ ,  $W2(4.6\mu\text{m})$ ,  $W3(12\mu\text{m})$ ,  $W4(22\mu\text{m})$ , and sources were selected using  $W1$  and  $W2$  due to their superior depth. We use the catalog constructed by Secrest et al. [1]. The data set comprises 1,355,352 quasars selected from the CatWISE2020 catalog. The selection focuses primarily on emission at wavelengths of  $3.4\mu\text{m}$  ( $W1$ ) and  $4.6\mu\text{m}$  ( $W2$ ) with a color cut of  $W1 - W2 > 0.8$  applied to ensure that AGN-dominated emission follows a power-law distribution. By cross-correlating the quasar sample with the eBOSS sample [45], it was found that the CatWISE data has a mean redshift of  $z \sim 1.2$  [1], making it largely insensitive to local bulk velocity effects.

The quasars are binned into a HEALPix<sup>3</sup> [46] map with  $N_{\text{side}} = 64$ ; the mean subtracted data is presented in the left panel of Figure 1. The same data, tophat smoothed with

<sup>2</sup>The velocity and direction of this dipole are  $v_{\text{pec}} = 369.82 \pm 0.11 \text{ km s}^{-1}$ ,  $(\ell, b) = (264.02^\circ, 48.25^\circ)$  in galactic coordinates, assuming that it is purely kinematic [29, 30].

<sup>3</sup><http://healpix.sourceforge.net>

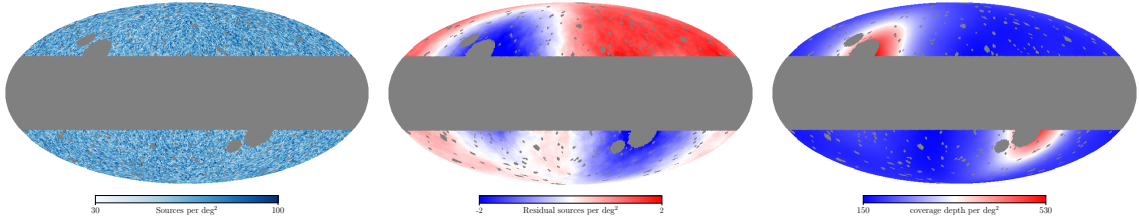


**Figure 1:** [Left panel] CatWISE quasar data binned into a  $N_{\text{side}} = 64$  HEALPix map, unsmoothed and mean subtracted. [Middle panel] The same data as in the left panel, but now smoothed using a tophat filter of area 1 steradian. [Right panel] The W1 coverage map, also smoothed with a 1 steradian tophat.

smoothing area 1 steradian, is presented in the middle panel and the W1 coverage depth of the survey, also smoothed over 1 steradian, is presented in the right panel. The quasar distribution presents a clear correlation with the scanning of the telescope. We discuss the removal of this effect in Section 4.3.

The grey regions in Figure 1 are masked. We use the same mask adopted in (Secrest et. al), which cuts all sources below  $|b| < 30^\circ$  and removed areas of poor photometry or artifacts using masks of radius  $< 2^\circ$ . Additionally, it also masks the Magellanic Clouds and Andromeda. In total, 291 regions in the sky, excluding the galactic plane, have been removed from the analysis. In an attempt to minimize any potential bias, we apply both the mask and antipodal image (in galactic coordinates) to the data. This is because one of the statistics that we measure is defined as the difference in density between antipodal points, and we want to avoid ambiguous situations where one pixel is masked<sup>4</sup>. In total, 54% of the sky is masked in our analysis. The data is corrected further by subtracting the CMB dipole and also a quadrupole that is assumed to be due to the scanning strategy of the telescope. These steps are documented in Section 4.

If the sources that we are measuring exhibit a power law spectral energy distribution  $S \propto \nu^\alpha$ , and the cumulative number count as a function of limiting flux density has the form  $N(> S) \propto S^{-x}$ , then our peculiar motion (magnitude  $v$ ) with respect to the assumed isotropic sample will generate a dipole in the observed number count of magnitude

$$\mathcal{D} = [2 + x(1 + \alpha)] \frac{v}{c} + \mathcal{O}\left(\frac{v^2}{c^2}\right). \quad (2.1)$$

Any flux limited sample with the above properties can therefore be used to test statistical isotropy, and specifically the standard model posits that any distant collection of objects should be at rest with respect to CMB photons, such that  $v \simeq 369.82 \text{ km s}^{-1}$  in equation (2.1). This was first discussed by Ellis and Baldwin [47] and is a generic prediction for isotropic cosmological models.

### 3 Methodology

In this Section we review the summary statistics that we extract from the quasar data, and how they can be used to determine the nature and significance of large scale features in the

<sup>4</sup>The additional masking does not significantly affect our conclusions. This is expected because the original mask is almost entirely antipodally symmetric (the galactic plane) and the other features; most notably LMC and SMC, are small in angular extent relative to the smoothing scales adopted in this work

catalog.

To quantify the level of anisotropy in the quasars, we create a smoothed residual map of the data. Statistical measures are computed from these residuals and their significance is evaluated against mock datasets that assume isotropy. This study focuses on two specific summary statistics: the  $Q$ - and the  $T$ -measures. To compute these quantities, we start by defining a field  $Q(\theta, \phi)$ , which is generated by smoothing the quasar number density. The procedure for this computation is outlined below:

1. **Construct a density map:** Create a density map by binning the quasars into a Healpix map. The monopole is subtracted from the map to obtain the residuals, which are represented as:

$$q(\hat{n}) = q_0(\hat{n}) - \bar{q}, \quad (3.1)$$

where  $q_0(\hat{n})$  is the original density, and  $\bar{q}$  is the mean density value.  $\hat{n}$  is the unit-normal pointing to the pixels.

2. **Generate a mask:** Generate a binary mask,  $m(\hat{n})$ , at the same resolution as the density map.
3. **Compute the smoothed data values:** For each unmasked pixel in the density map, calculate the smoothed value,  $Q_{\text{data}}$ , using a specified smoothing width,  $\delta$ , as follows:

$$Q_{\text{data}}(\theta, \phi; \delta) = \sum_{i=1}^N q_i(\theta_i, \phi_i) W(\theta, \phi, \theta_i, \phi_i; \delta), \quad (3.2)$$

$$W(\theta, \phi, \theta_i, \phi_i; \delta) = \frac{1}{\sqrt{2\pi}\delta} \exp \left[ -\frac{L(\theta, \phi, \theta_i, \phi_i)^2}{2\delta^2} \right] \Theta(\delta - L), \quad (3.3)$$

where the angular distance  $L(\theta, \phi, \theta_i, \phi_i)$  between pixel at angular position  $(\theta, \phi)$  and the  $i^{\text{th}}$  pixel at  $(\theta_i, \phi_i)$  is given by:

$$L(\theta, \phi, \theta_i, \phi_i) = 2 \arcsin \frac{R}{2}, \quad (3.4)$$

$$R = \left[ \sin(\theta_i) \cos(\phi_i) - \sin(\theta) \cos(\phi) \right]^2 \quad (3.5)$$

$$+ \left[ \sin(\theta_i) \sin(\phi_i) - \sin(\theta) \sin(\phi) \right]^2 \quad (3.6)$$

$$+ \left[ \cos(\theta_i) - \cos(\theta) \right]^2 \Big)^{1/2}, \quad (3.7)$$

and the step function is defined as  $\Theta(\delta - L) = 1$  if  $L < \delta$  and zero otherwise.

4. **Compute the smoothed mask values:** Similarly, calculate the smoothed mask value,  $Q_{\text{mask}}$ , for each pixel using the same smoothing width:

$$Q_{\text{mask}}(\theta, \phi; \delta) = \sum_{i=1}^N m_i(\theta_i, \phi_i) W(\theta, \phi, \theta_i, \phi_i; \delta). \quad (3.8)$$

5. **Calculate the scaled  $Q$ -value:** Normalize the smoothed data values by the smoothed mask values to compute the scaled  $Q$ -value:

$$Q_{\text{scaled}} = \frac{Q_{\text{data}}}{Q_{\text{mask}}}. \quad (3.9)$$

6. **Calculate the  $T$ -value:** The field  $T(\theta, \phi)$  is defined as the difference between the  $Q$ -value at a given pixel and the  $Q$ -value at its antipodal pixel

$$T(\hat{n}) = Q_{scaled}(\hat{n}) - Q_{scaled}(-\hat{n}). \quad (3.10)$$

The method is straightforward and in this context describes the generation of a smoothed density field from a pixelated map in real space. It has been more generally used to search for anisotropic signals in sparse data [12, 18]. The particular smoothing kernel adopted in this work is a product of a top hat and Gaussian. We selected Gaussian smoothing because it weights pixels by separation, but when selecting large  $\delta \sim \pi/2$  scales the Gaussian kernel can over-smooth the field, potentially washing out the largest scale feature in the data (a dipole). This motivates the implementation of a top hat cut at  $L = \delta$ .

From the  $Q$  map constructed above, we find the maximum  $Q_{\max}$  and minimum  $Q_{\min}$  values and also the maximum  $T_{\max}$  of the  $T$  map; it is these statistics that will be used to quantify the magnitude and significance of features in the data as a function of scale  $\delta$ . Evaluating the significance of extreme values of a density field is a well established methodology in cosmology [12, 18]. In  $Q_{\min}$  and  $Q_{\max}$ , we are studying the one-point statistics of the field.  $T_{\max}$  is a two-point statistic, but is sensitive only to odd, large-scale multipoles. The relative location of  $Q_{\max}$ ,  $Q_{\min}$  and  $T_{\max}$  on the sphere provides additional information about the nature of the density field. If a dipole dominates the large scale modes, one would expect  $Q_{\max}$  and  $Q_{\min}$  to be antipodal and aligned with the  $T_{\max}$  direction.

To determine the statistical significance of  $Q_{\max}$ ,  $Q_{\min}$  and  $T_{\max}$ , we need to calculate these same statistics for a set of isotropic mock data. To do so we generate  $N_{\text{real}} = 10^5$  mock realisations, in which the original  $q(\hat{n})$  quasar map is randomly scattered into the unmasked pixels and  $Q_{scaled}$  and  $T$  maps are constructed using the smoothing algorithm above.  $Q_{\max}$ ,  $Q_{\min}$  and  $T_{\max}$  are extracted from each random, isotropic realisation and a probability distribution is generated. The statistical significance of the measured  $Q_{\max}$ ,  $Q_{\min}$ ,  $T_{\max}$  values are inferred from these mock probability distributions. The procedure is repeated for various smoothing scales  $\pi/2 \leq \delta \leq \pi/16$ .

From the  $Q$  maps, we also extract the two-point angular correlation function to highlight the dominant large scale features in the data. The Landy-Szalay (LS) estimator [48] is a widely used and robust method for calculating the angular two-point correlation function, and is given by

$$\zeta(\theta) = \frac{DD(\theta) - 2DR(\theta) + RR(\theta)}{RR(\theta)}, \quad (3.11)$$

where  $DD$  is the number of data-data pairs at angular separation  $\theta$ ,  $DR$  is the number of data-random pairs and  $RR$  is the number of random-random pairs. The random catalogs are generated by scattering the residual pixels ( $q$ ) on the sphere while preserving the mask. The estimator minimizes edge effects and biases present in simpler estimators, and also has lower variance compared to other estimators.

## 4 Results

In this section, we present the findings of our analysis. Using the methodology outlined in Section 3, we systematically examine the quasar datasets by sequentially removing known signals from the complete dataset and analyzing the resulting density maps.

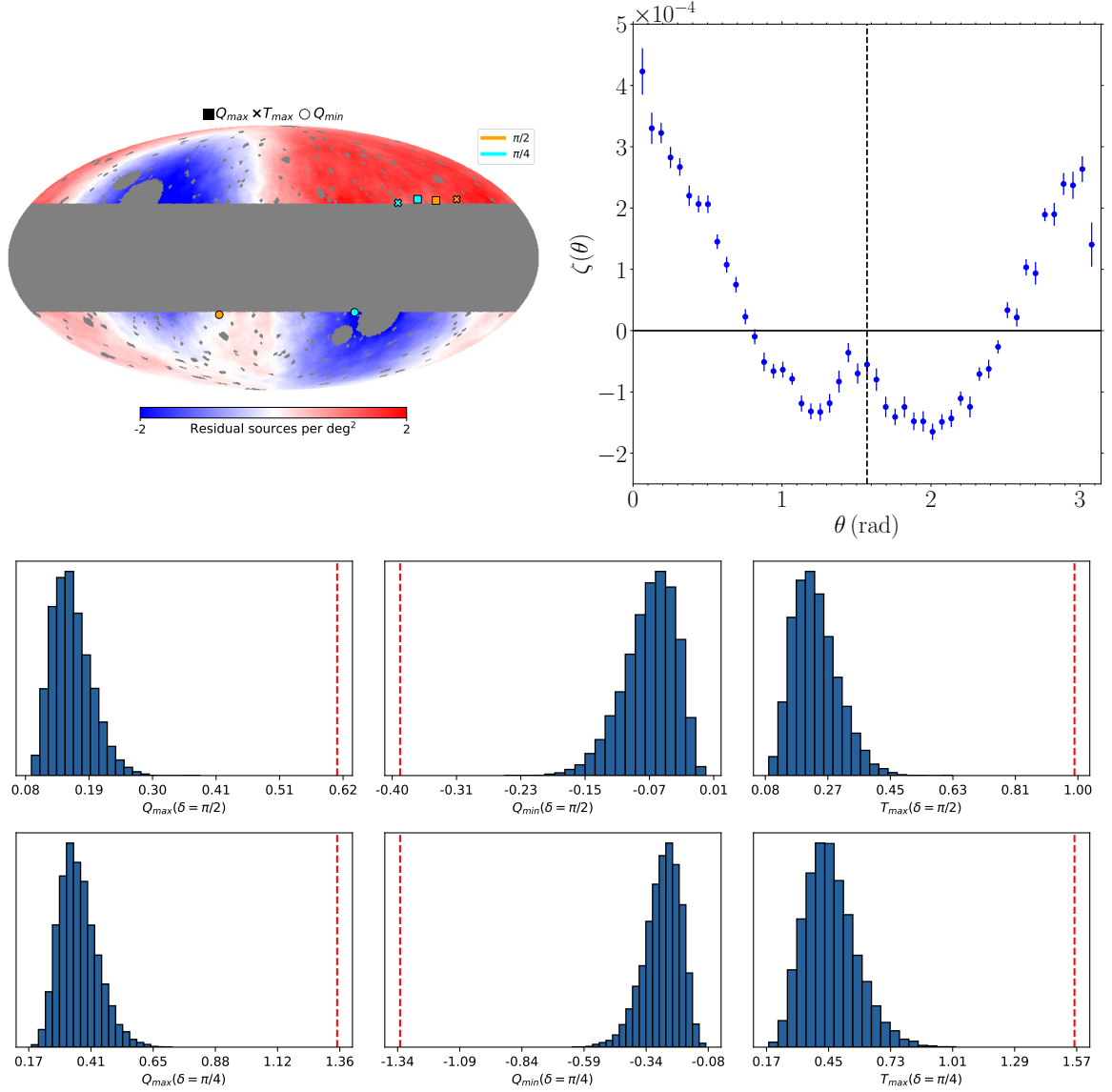


**Figure 2:** Results from the real-space analysis of the full data density map. **Top Left:** The smoothed density map of the quasar distribution from the CatWISE catalog. The gray regions represent masked areas in the map. **Top Right:** The angular correlation function,  $\zeta(\theta)$ , where  $\theta$  is in radians. The shape is predominantly quadrupolar but is modulated by a dipole. **Bottom Rows:** The distributions of  $Q_{\max}$ ,  $Q_{\min}$  and  $T_{\max}$  from the mock catalog are shown alongside the corresponding values from the data. Results are presented for two smoothing scales:  $\delta = \pi/2$  (middle row) and  $\delta = \pi/4$  (bottom row).

#### 4.1 Full Data Density Map

The analysis of the complete, unmodified CatWISE dataset is presented in Figure 2. This dataset predominantly exhibits two signals: a dipole and a quadrupole. In the top left panel we present the smoothed density field on the sky, in the top right panel the angular correlation function, and in the lower panels the statistics  $Q_{\max}$ ,  $Q_{\min}$  and  $T_{\max}$  (left, middle,

right columns) for two smoothing scales;  $\delta = \pi/2$  (top row) and  $\delta = \pi/4$  (bottom row). The vertical red dashed lines are the values of the statistics extracted from the data, and the blue histograms are  $N = 10^5$  isotropic realisations that we use to determine the statistical significance. The angular correlation function clearly identifies a strong quadrupole signal, that is modulated by a dipole. The latter manifests as an amplitude difference between the maxima of the angular correlation function. There is also a feature in the form of a bump at angular separations  $\theta \sim \pi/2$ .

We find a significant dipole signal using  $Q_{\max}$ ,  $Q_{\min}$  and  $T_{\max}$  at a smoothing width of  $\delta = \pi/2$ . This dipole signal is typically associated with the relative motion of the observer with respect to the CMB rest frame. At a reduced smoothing width of  $\delta = \pi/4$  (bottom panels), we observe that the data values of  $Q_{\max}$  and  $Q_{\min}$  move further away from the isotropic histograms – indicating increased significance – while  $T_{\max}$  remains practically unchanged. This behavior confirms the presence of a quadrupole signal in addition to the dipole within the data set;  $Q_{\max}$  and  $Q_{\min}$  are local features that are sensitive to the presence of the quadrupole which is dominant for  $\delta = \pi/4$ , whilst  $T_{\max}$  is only sensitive to the dipole on these smoothing scales. For both  $\delta = \pi/2$  and  $\pi/4$ , we find zero isotropic realisations that generate  $Q_{\max}$ ,  $Q_{\min}$  or  $T_{\max}$  that are comparable to the data. This first case simply serves as a validation of our methodology; visual inspection of the map shows that it is dominated by a quadrupole.

## 4.2 Full Data Density Map After Removing the CMB Dipole Signal

The quasar map contains at least one large-scale feature that is expected within the standard model; our velocity with respect to the CMB, and presumably large scale structure, should generate a dipole in the number count [47]. To further isolate signals, we subtract the CMB dipole contribution from the full dataset and repeat the analysis. The method by which we subtract the dipole is described in [subsection A.1](#). The results are presented in [Figure 3](#); the panels show the same quantities as in [Figure 2](#). The angular correlation function reveals a strong quadrupole signal alongside a much reduced, but still non-zero, dipole modulation. The quadrupole is clearly still the dominant signal in the map.

In the lower panels, we see that upon removing the CMB dipole signal the significance of  $Q_{\max}$ ,  $Q_{\min}$  and  $T_{\max}$  decreases at  $\delta = \pi/2$ . At  $\delta = \pi/4$ ,  $Q_{\max}$  and  $Q_{\min}$  remain highly significant  $p \ll 1$ , while  $T_{\max}$  shows a reduced significance of approximately  $p \sim 0.01$ . This difference arises because on large scales  $T_{\max}$  is sensitive solely to a dipole signal, and the dominant dipole component, the CMB dipole, has been removed. The remaining significant signal may be attributed to an excess dipole intrinsic to the quasar dataset.  $Q_{\min}$  and  $Q_{\max}$  are sensitive to the quadrupole and remain highly significant, with zero isotropic realisations being found with comparable values to the data.

## 4.3 Ecliptic-Corrected Density Map

The presence of a quadrupole is well known, and is typically attributed to the scanning strategy of the telescope. We correct for the ecliptic scanning pattern of WISE as described in [1, 33]; the quasar number count varies approximately linearly with ecliptic latitude. The data is binned in ecliptic latitude, a linear curve (slope=  $-0.051$ , intercept=  $68.89 \text{ deg}^{-2}$ ) is fitted to the number counts, and sources are artificially added to the map to remove the linear systematic variation. The result of this procedure is presented in [Figure 4](#). The density map (top left panel) still presents large scale modes, most clearly a prominent dipole signal.

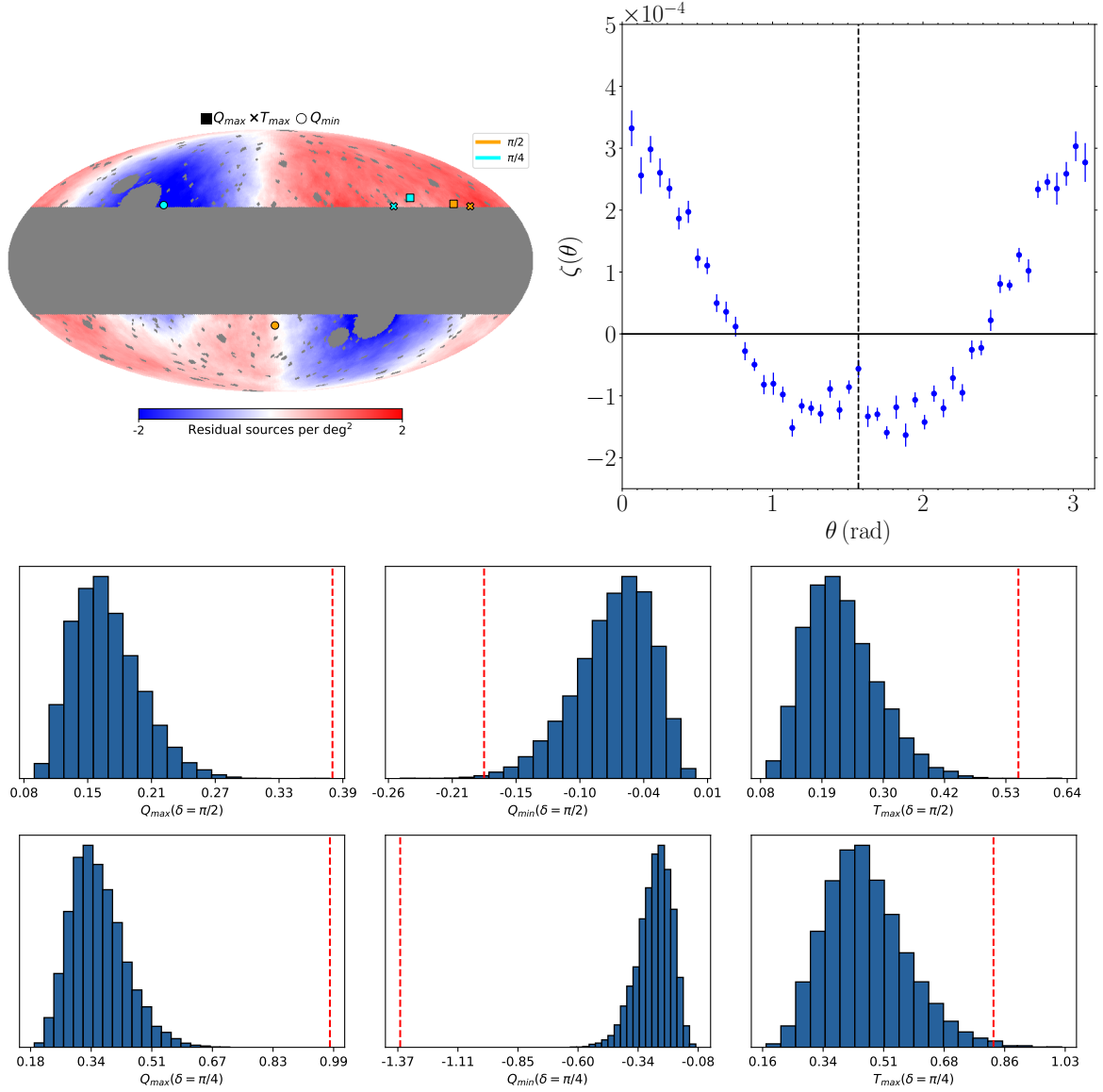


**Figure 3:** Results from the real-space analysis of the CMB dipole-removed density map. **Top Left:** The smoothed density map of the quasar distribution from the CatWISE catalog. The gray regions represent masked areas in the map. **Top Right:** The angular correlation function,  $\zeta(\theta)$ , where  $\theta$  is in radians. The shape is now predominantly quadrupolar. **Bottom Rows:** The distributions of  $Q_{\max}$ ,  $Q_{\min}$  and  $T_{\max}$  from the mock catalog are shown alongside the corresponding values from the data. Results are presented for two smoothing scales:  $\delta = \pi/2$  (middle row) and  $\delta = \pi/4$  (bottom row).

This is partly due to the CMB dipole, which is also identified in the correlation function (top right panel).

The  $Q_{\min}$ ,  $Q_{\max}$  and  $T_{\max}$  statistics are now consistent with the dominance of a dipole signal. At  $\delta = \pi/2$  smoothing,  $Q_{\max}$ ,  $Q_{\min}$  and  $T_{\max}$  each exhibit high significance. At  $\delta = \pi/4$ , the significance of the data relative to the mocks shows no notable change. If a

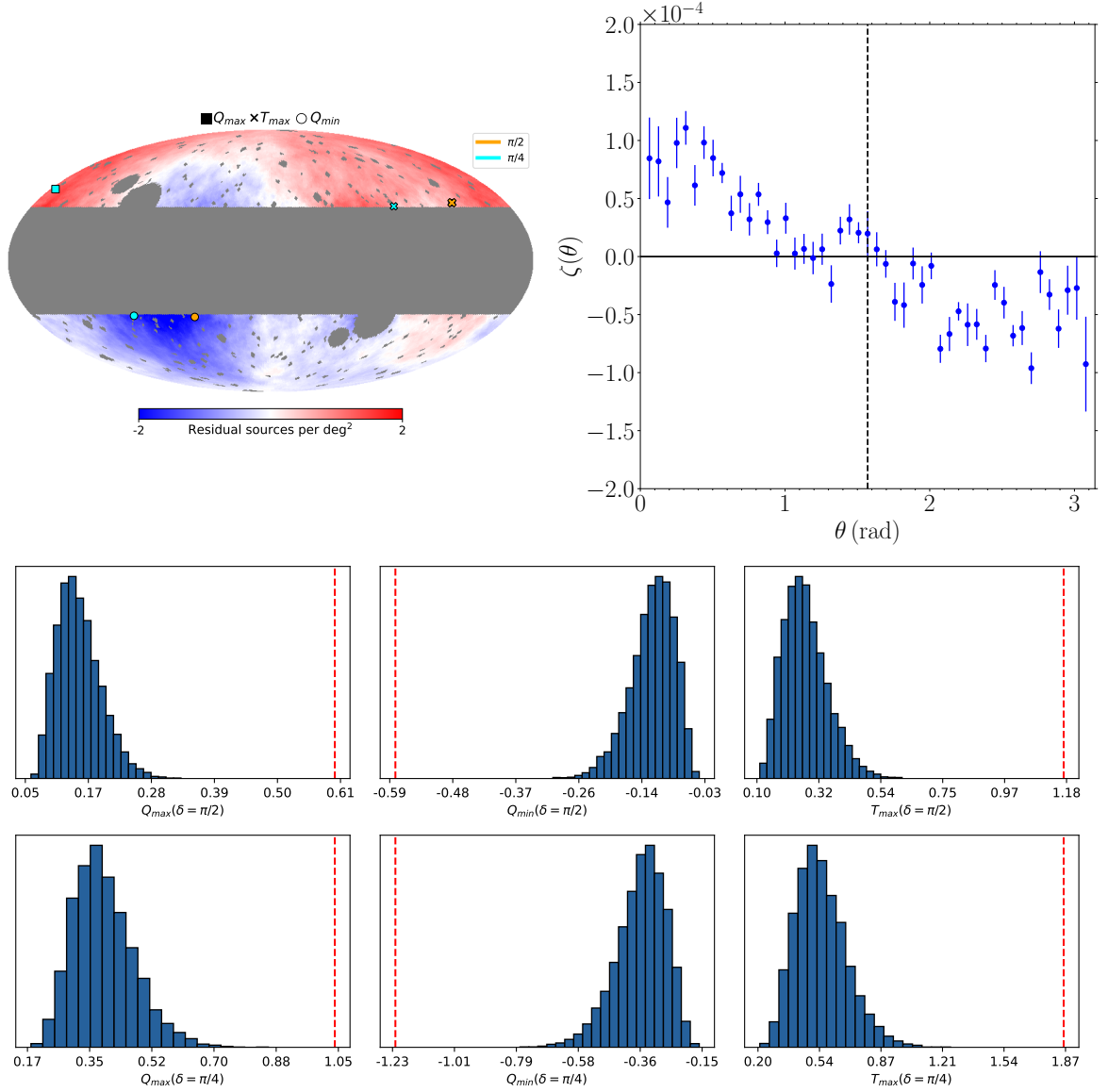


**Figure 4:** Results from the real-space analysis of the ecliptic-corrected density map. **Top Left:** The smoothed density map of the quasar distribution from the CatWISE catalog. The gray regions represent masked areas in the map. **Top Right:** The angular correlation function,  $\zeta(\theta)$ , where  $\theta$  is in radians. The shape is predominantly dipolar. **Bottom Rows:** The distributions of  $Q_{\max}$ ,  $Q_{\min}$  and  $T_{\max}$  from the mock catalog are shown alongside the corresponding values from the data. Results are presented for two smoothing scales:  $\delta = \pi/2$  (middle row) and  $\delta = \pi/4$  (bottom row).

$\sim \pi/4$  feature was present in the map, then we would observe a change in the significance of  $Q_{\max}$  and  $Q_{\min}$  relative to the  $\pi/2$  smoothing, but not in  $T_{\max}$ . The fact that we observe no significant change in the significance of any of the statistics indicates that the quadrupole signal has been successfully removed by the ecliptic correction. The exact reason why the data should be cleaned in this way, and why there is a linear relation between the number

counts as a function of ecliptic latitude, is uncertain. Stellar contamination has been proposed as an explanation [26], or alternatively bright obfuscating faint sources in regions where the highest number of observations are made.

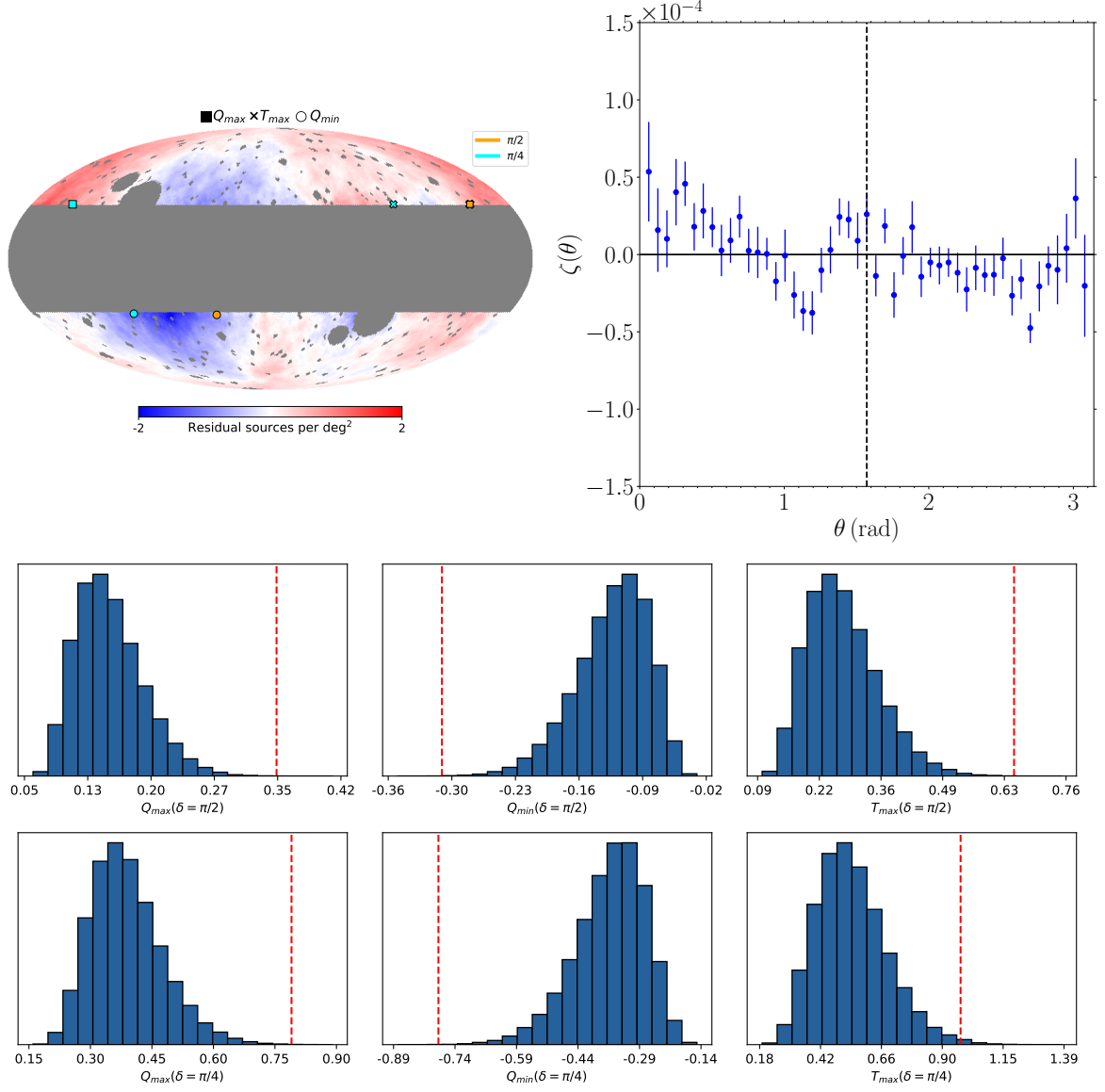


**Figure 5:** Results from the real-space analysis of the CMB dipole-removed and ecliptic-corrected density map. **Top Left:** The smoothed density map of the quasar distribution from the CatWISE catalog. The gray regions represent masked areas in the map. **Top Right:** The angular correlation function,  $\zeta(\theta)$ , where  $\theta$  is in radians. **Bottom Rows:** The distributions of  $Q_{\max}$ ,  $Q_{\min}$  and  $T_{\max}$  from the mock catalog are shown alongside the corresponding values from the data. Results are presented for two smoothing scales:  $\delta = \pi/2$  (middle row) and  $\delta = \pi/4$  (bottom row).

#### 4.4 Ecliptic-Corrected & CMB Dipole Removed Density Map

Finally, we remove the CMB dipole signal from the ecliptic-corrected density map and reanalyze the data using the previously described methods. The results are shown in Figure 5. Assuming we have successfully removed observational systematics, then the map (top left panel) should be statistically isotropic according to the standard cosmological model. However, after removing all known signals, residual large scale features are identified both in the density map and angular correlation function (top right panel). This signal, first observed in [1], could be attributed to anomalous dipole, which indicates that large scale structure does not occupy a common rest frame with the CMB temperature field. Our measurement of the angular correlation function of the data (top right panel) also presents a large scale dipole, whilst retaining a feature at  $\theta \sim \pi/2$ .

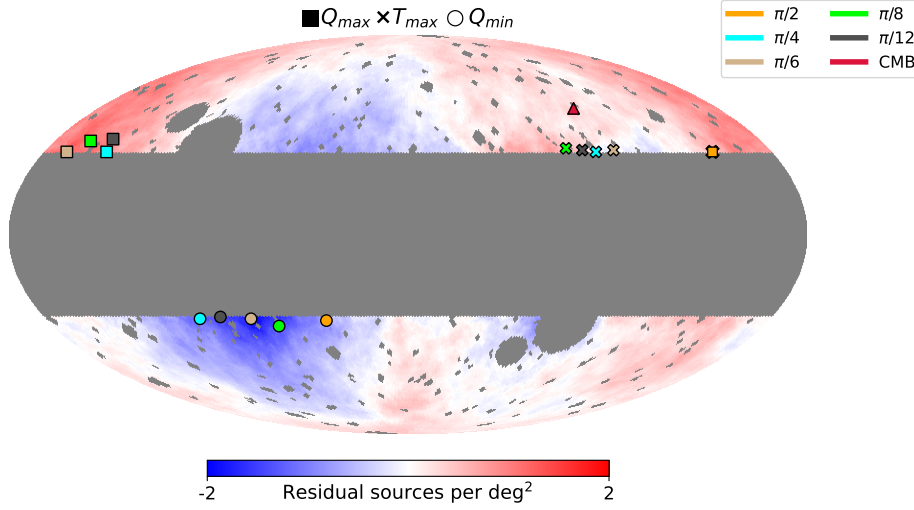


**Figure 6:** The directions of  $Q_{\max}$ ,  $Q_{\min}$  and  $T_{\max}$  on the sky, inferred from the ecliptic corrected, CMB dipole subtracted map smoothed over different scales. The squares/crosses/circles represent  $Q_{\max}/T_{\max}/Q_{\min}$ , respectively. Results are presented for various smoothing scales from  $\delta = \pi/2$  to  $\pi/12$ , using different colors. The quantities  $Q_{\min}$  and  $T_{\max}$  are close to antipodal for most smoothing scales selected. The red triangle denotes the CMB dipole direction. The color map is the quasar data smoothed with a tophat of area 1 steradian, and is underplotted for reference.

	$\pi/2$	$\pi/4$	$\pi/6$	$\pi/8$	$\pi/12$	$\pi/16$
$Q_{\max}$	0.00004	0.00026	0.0046	0.06	0.36	0.23
$Q_{\min}$	0.0002	0.0002	<0.00001	0.0005	0.03	0.091
$T_{\max}$	0.0002	0.0054	0.0011	0.0057	0.0278	0.245

**Table 1:**  $p$ -values for  $Q_{\max}$ ,  $Q_{\min}$  and  $T_{\max}$  of the field for various different smoothing scales  $\pi/16 \leq \delta \leq \pi/2$ . When smoothing on the largest scales, a dipole is clearly observed at high significance. As we decrease the smoothing, the minimum value of the field  $Q_{\min}$  becomes the most significant feature in the map, down to  $\delta = \pi/8$ . As we continue to decrease  $\delta$ , the data becomes consistent with random fluctuations ( $p$ -values  $> 0.02$ ).

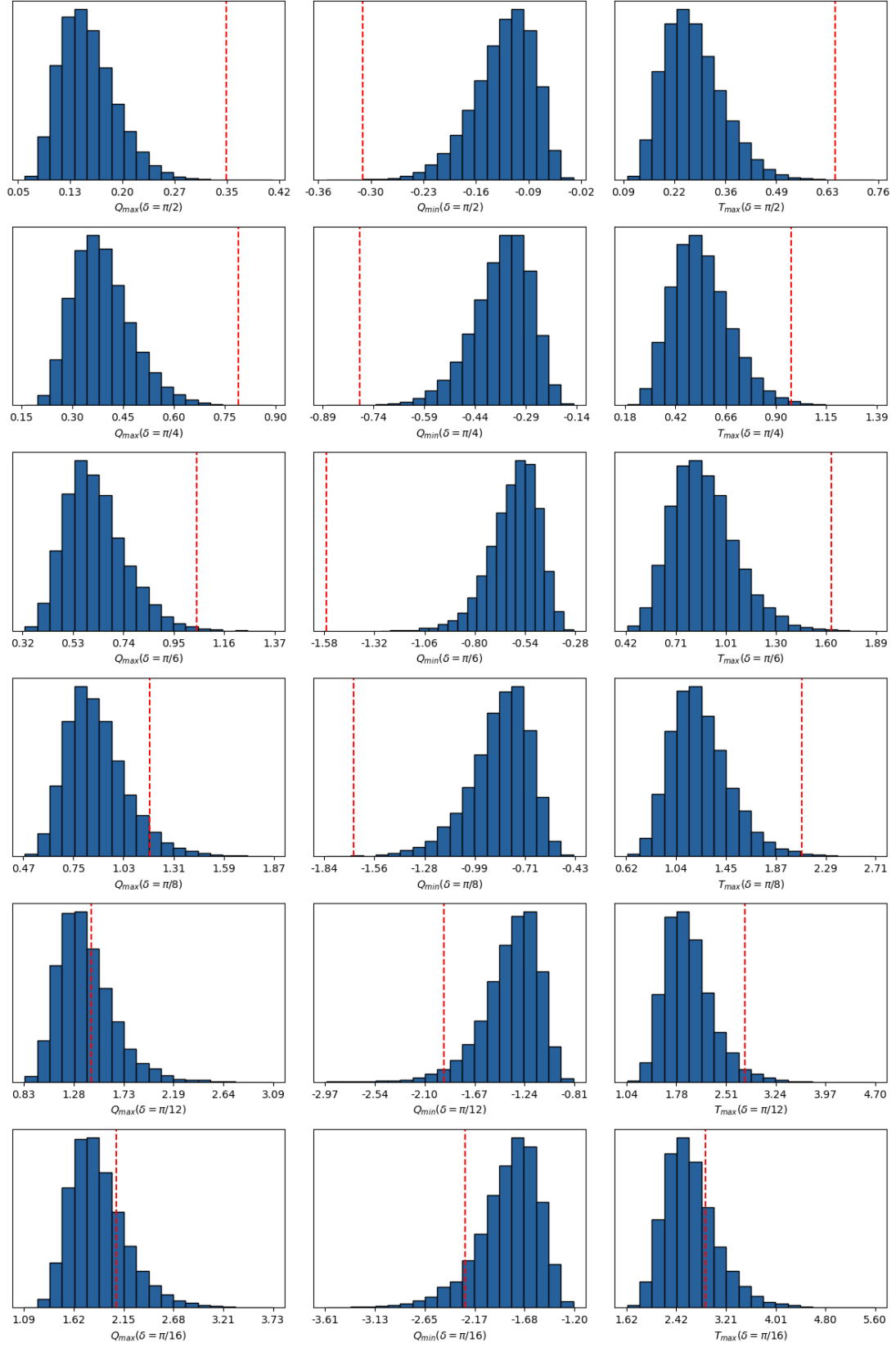


**Figure 7:** The distributions of  $Q_{\max}$ ,  $Q_{\min}$  and  $T_{\max}$  from the mock catalog are shown alongside the corresponding values from the data for  $\delta = \pi/2$  to  $\pi/16$ .

Following the application of the ecliptic correction and the removal of the CMB dipole signal, the statistical significance of  $Q_{\max}$ ,  $Q_{\min}$ , and  $T_{\max}$  decrease markedly in comparison to the full density map. This is expected; we have removed the two largest sources of anisotropy. At both smoothing widths examined, the significance of  $Q_{\max}$  and  $T_{\max}$  are practically the same, suggesting that the residual signal contains no significant quadrupolar contribution. These findings are presented in the middle and lower panels of [Figure 5](#).

We studied the map and associated summary statistics as a function of the smoothing scale  $\delta$ . As we decrease  $\delta$ , small scale modes will become increasingly dominant. If the anomalous signal in the data is due to large scale modes, then we can expect the significance of  $Q_{\max}$ ,  $Q_{\min}$  and  $T_{\max}$  to decrease with  $\delta$ . With this in mind, we apply smoothing at various scales down to  $\delta = \pi/16$  and compute  $Q_{\max}$ ,  $Q_{\min}$  and  $T_{\max}$  summary statistics. The distributions of  $Q_{\max}$ ,  $Q_{\min}$  and  $T_{\max}$  for different smoothing scales are presented in [Figure 7](#) and the corresponding p-values of the data values relative to the random realisations are summarized in [Table 1](#). We note that the probability distributions are skewed, non-Gaussian and therefore we do not quote our results in terms of standard deviations.

The statistical significance of  $Q_{\max}$ ,  $Q_{\min}$  and  $T_{\max}$  extracted from the data decreases with the decreasing smoothing scale, indicating that only the largest scales are anomalous. We find that  $Q_{\min}$  presents the most significant feature in the data, and its significance peaks at smoothing scale  $\delta = \pi/6$ . We can see in the density map (cf top left panel of [Figure 5](#)) that the under-density in the south sky is relatively localized compared to the overdense regions in the north, which are more diffuse. It is  $Q_{\min}$  that drives the significance of  $T_{\max}$  on scales  $\delta \sim \pi/6$ ; the fact that the significance of  $T_{\max}$  is lower than  $Q_{\min}$  indicates that a dipole is not the only feature in the data at these scales. As we decrease  $\delta$  to values  $< \pi/8$ , the significance of all features in the data becomes negligible. This is expected, the small scale features in the map should be consistent with random fluctuations<sup>5</sup>.

#### 4.5 Ecliptic-Corrected & Anomalous Dipole Removed Density Map

The final case that we consider is the quasar map after it has been ecliptic corrected and the anomalous dipole inferred in [\[1\]](#) removed;  $\mathcal{D} = 0.01554$ ,  $(b, \ell) = (28.8^\circ, 238.2^\circ)$ . There is currently no theoretically compelling explanation for the existence of such a dipole; it is an empirical fit to the data after the quadrupole has been corrected. In this section, we determine the extent to which a pure dipole can remove the large scale anisotropic features from the ecliptic corrected map. The results are presented in [Figure 8](#).

In the top left panel, we still observe some large scale features in the map, including the southern underdense region. This underdense region is now surrounded by overdense patches, and the northern sky in the antipodal direction to  $Q_{\min}$  is now underdense. Both effects are a result of the dipole being an imperfect subtraction of the large scale features. We have shown that the significance of  $Q_{\min}$  peaks when we smooth at  $\delta = \pi/6$ , whereas a dipole subtraction will modify the density field on scales  $\sim \pi/2$ . This is the reason why regions in the vicinity of  $Q_{\min}$  now exhibit more pronounced overdensities. We have also found that  $Q_{\max}$  is not typically antipodal to  $Q_{\min}$ , and so the dipole subtraction over-compensates in the north sky and creates a new large-scale underdensity. However, in spite of these issues we note that the removal of the anomalous dipole has isotropized the map to a much higher degree than the CMB dipole subtraction in the previous section; the data are now mostly consistent with the random isotropic realisations as shown by the histograms in the lower

<sup>5</sup>There is clustering information in the quasar distribution [\[49\]](#), but we do not expect a significant correlation for the pixel sizes and smoothing scales selected in this work.

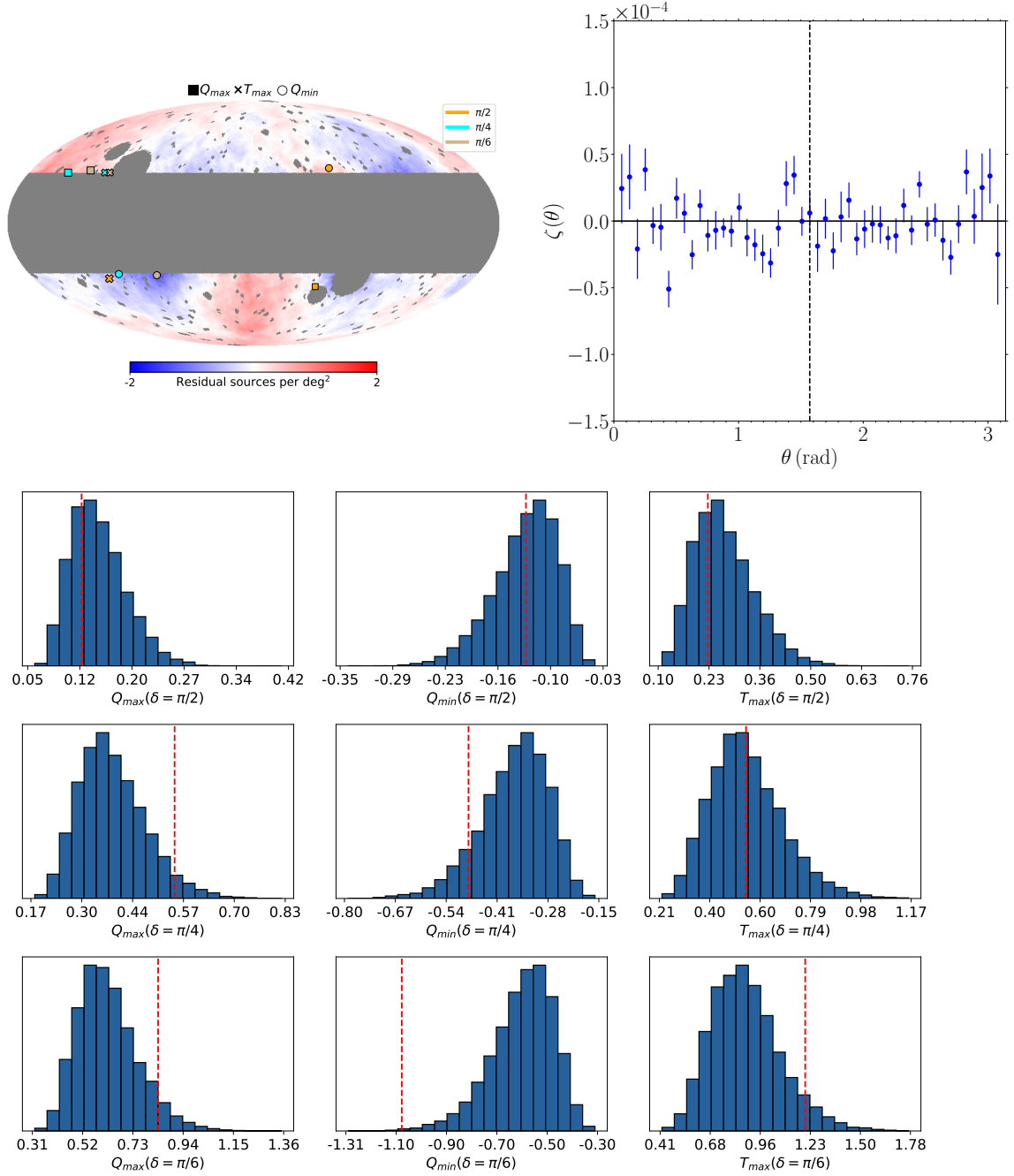


**Figure 8:** Results from the real-space analysis of the ecliptic-corrected and anomalous dipole removed density map. **Top Left:** The smoothed density map of the quasar distribution from the CatWISE catalog. The gray regions represent masked areas in the map. **Top Right:** The angular correlation function,  $\zeta(\theta)$ , where  $\theta$  is in radians. **Bottom Rows:** The distributions of  $Q_{\max}$ ,  $Q_{\min}$  and  $T_{\max}$  from the mock catalog are shown alongside the corresponding values from the data. Results are presented for three smoothing scales:  $\delta = \pi/2$  (top) and  $\delta = \pi/4$  (middle) and  $\delta = \pi/6$  (bottom).

panels. The only residual anisotropy of significance is  $Q_{\min}$  when the map is smoothed at  $\pi/6$  (cf. bottom middle panel) with corresponding p-value  $p = 0.0018$ . This is the same underdensity as found in the previous subsection. It remains present in the map, but with much reduced significance, because part of the signal has been attributed to the dipole and removed.

## 5 Discussion

In this study, we generated smoothed density fields from CatWISE data and extracted the summary statistics  $Q_{\max}$ ,  $Q_{\min}$ , and  $T_{\max}$ . By comparing these values to those obtained from isotropic mock realizations, we assessed the statistical significance of anisotropy in the data across different smoothing scales. After accounting for known sources of anisotropy, we identified a residual anisotropic signal whose significance decreased as the smoothing width was reduced.

The quantities  $Q_{\max}$  and  $Q_{\min}$  are one-point functions, while  $T_{\max}$  is a two-point function restricted to antipodal points on the sphere. Since our summary statistics differ from those used in previous studies, we do not expect to obtain the same statistical significance as dedicated dipole searches. In particular,  $Q_{\min}$  and  $Q_{\max}$  are local quantities that are not uniquely sensitive to a dipole. Conversely,  $T_{\max}$  is sensitive to odd-multipole modes. Our results indicate the presence of a large-scale underdense feature in the southern sky and more dispersed overdense patches in the north. Together, these features reveals the presence of a significant dipole ( $Q_{\min}$  and  $Q_{\max}$  are antipodal and both align with  $T_{\max}$ ) when the density field is smoothed on large scales ( $\delta \simeq \pi/2$ ). However, when smoothed at  $\delta \simeq \pi/2$ , smaller scale modes will be generically suppressed relative to the dipole, and  $Q_{\min}$ ,  $Q_{\max}$  are more likely to be antipodally located. On smaller scales, the underdense patch remains significant down to  $\delta \sim \pi/8$  but  $Q_{\min}$  and  $Q_{\max}$  are no longer antipodal. As the smoothing width decreases further to  $\delta \lesssim \pi/8$ , the data becomes fully consistent with isotropic, random realizations. Additionally,  $T_{\max}$  is located in the region antipodal to  $Q_{\min}$  but not  $Q_{\max}$ , suggesting that  $T_{\max}$  is predominantly driven by a minimum rather than a maximum-minimum pair in the smoothed data. Notably, we find a high significance for  $Q_{\min}$  at a smoothing width of  $\delta = \pi/6$  (p-value  $<< 10^{-5}$ ), pointing to the presence of a localized underdensity in the data of characteristic size  $\sim \pi/6$  in the direction  $(b, \ell) = (-31^\circ, 78^\circ)$ , with antipodal point  $\sim (31^\circ, 258^\circ)$ . For comparison, if we smooth on large scales  $\delta = \pi/2$ , we find that  $Q_{\min}$  is antipodal to  $Q_{\max}$  with the latter located at  $(b, \ell) = (30^\circ, 210^\circ)$ , in reasonable agreement with the result of [1].

Finally, we measured the same statistics after removing the anomalous dipole inferred in [1] from the ecliptic-corrected quasar map. The removal of this dipole isotropizes the data to a higher degree than the CMB dipole subtraction, but some residual large scale features remain. This is unavoidable; we have found that maximally anisotropic features are present when we smooth on smaller scales  $\delta \sim \pi/6$ , which implies that any dipole subtraction must be imperfect in resolving this anisotropy. Even so, the anomalous dipole correction reduces the significance of any additional anisotropic features to p-values  $p = 0.0018$ .

The method adopted in this work can only find extreme field values in the ‘direction of unmasked pixels’; if the data contains a dipole that peaks within the mask then our approach will yield a biased estimate of the true direction. Different methods, such as directly fitting

a dipole, can infer a preferred direction within masked regions<sup>6</sup>. However, our intention is not to specifically search for a dipole or even to find the preferred direction of any signal. Rather, our methodology is an attempt to search for anomalies in a model independent manner, by evaluating the significance of extreme values of the density field after smoothing at various scales. The method that we have adopted takes extreme values of the smoothed quasar density field on the sphere, and compares them to the same quantities extracted from isotropic random resampling of the data. The methodology can be used to test for dipoles and other large scale modes, by comparing the direction and magnitude of  $Q_{\max}$ ,  $Q_{\min}$  and  $T_{\max}$  as a function of smoothing scale.

The quasar data contains large scale modes that are statistically rare compared to random, isotropic re-sampling of the same data. The exact nature and origin of these modes, and whether they are sourced by unknown systematics or physical effects beyond the standard cosmological model, remains an open question and will require future study. Of particular interest is the determination of the redshift dependence of the signal, and also its sensitivity to other properties of the data – brightness, color etc. Confirming the signal in other data, such as done in [33], is also an important future goal. Finally, studying the properties of other large scale structure catalogs could shed more light on the structures found in this work.

## Acknowledgments

The authors would like to thank Roya Mohayaee, Subir Sarkar and Nathan Secrest for insightful discussions. AA and SA are supported by an appointment to the JRG Program at the APCTP through the Science and Technology Promotion Fund and Lottery Fund of the Korean Government, and were also supported by the Korean Local Governments in Gyeongsangbuk-do Province and Pohang City. SA also acknowledges support from the NRF of Korea (Grant No. NRF-2022R1F1A1061590) funded by the Korean Government (MSIT). A.S. would like to acknowledge the support by National Research Foundation of Korea 2021M3F7A1082056, and the support of the Korea Institute for Advanced Study (KIAS) grant funded by the government of Korea.

## A Appendix

### A.1 Removing a dipole signal from a radio source map

Ellis and Baldwin derived the dipole anisotropy in the number count of radio sources that are isotropically distributed when observed from a reference frame moving with velocity  $v$  [47]. Consider a population of radio sources with power-law spectra, given by  $S \propto \nu^{-\alpha}$ , and an integral source count distribution per unit solid angle expressed as  $\frac{dN}{d\Omega}(> S) \propto S^{-x}$ , above a limiting flux density  $S$ . When viewed from a moving reference frame with velocity  $v$ , this distribution exhibits a dipole anisotropy with an amplitude given by

$$\mathcal{D} = [2 + x(1 + \alpha)] \frac{v}{c}. \quad (\text{A.1})$$

Since our local frame moves with a velocity of  $v = 369$  km/s relative to the cosmic microwave background (CMB) rest frame, a dipole anisotropy of amplitude  $\mathcal{D}_{\text{CMB}} = 0.007$  is expected

---

<sup>6</sup>Direct fitting methods may also be prone to biases due to the presence of a mask and also due to prior assumptions made about the nature of the signal.

in the number count of radio sources, aligned with the direction of motion. To quantify any excess dipole signal, this CMB-induced dipole must be subtracted.

Given a full-sky distribution, a dipole anisotropy of amplitude  $\mathcal{D}$  along a direction  $\hat{d}$  can be introduced or removed using the transformation

$$S(\hat{n}) = S_0 \left( 1 \pm \mathcal{D} \hat{n} \cdot \hat{d} \right), \quad (\text{A.2})$$

where  $\hat{n}$  denotes the unit vector corresponding to a given sky position.

## References

- [1] N. J. Secrest, S. von Hausegger, M. Rameez, R. Mohayaee, S. Sarkar and J. Colin, *A test of the cosmological principle with quasars*, *The Astrophysical Journal Letters* **908** (2021) L51.
- [2] A. Hajian and T. Souradeep, *Measuring statistical isotropy of the CMB anisotropy*, *Astrophys. J. Lett.* **597** (2003) L5 [[astro-ph/0308001](#)].
- [3] Dipanshu, A. Karan and T. Souradeep, *Statistical Isotropy Violations in CMB Temperature Anisotropy: Analysis Using Minimal Bipolar Spherical Harmonics*, **2411.11139**.
- [4] T. Buchert, *On average properties of inhomogeneous fluids in general relativity. 1. Dust cosmologies*, *Gen. Rel. Grav.* **32** (2000) 105 [[gr-qc/9906015](#)].
- [5] T. Buchert and J. Ehlers, *Averaging inhomogeneous Newtonian cosmologies*, *Astron. Astrophys.* **320** (1997) 1 [[astro-ph/9510056](#)].
- [6] M. Gasperini, G. Marozzi, F. Nugier and G. Veneziano, *Light-cone averaging in cosmology: Formalism and applications*, *JCAP* **07** (2011) 008 [[1104.1167](#)].
- [7] D. B. H. Verweg, B. J. T. Jones and R. van de Weygaert, *Cosmic averaging over multiscaled structure: on foliations, gauges and backreaction*, **2409.00024**.
- [8] C. A. Meegan, G. N. Pendleton, M. S. Briggs, C. Kouveliotou, T. M. Koshut, J. P. Lestrade et al., *The third batse gamma-ray burst catalog*, *The Astrophysical Journal Supplement Series* **106** (1996) 65.
- [9] C. Blake and J. Wall, *A velocity dipole in the distribution of radio galaxies*, *Nature* **416** (2002) 150.
- [10] E. L. Wright et al., *The wide-field infrared survey explorer (wise): Mission description and initial on-orbit performance*, *Astron. J.* **140** (2010) 1868.
- [11] A. K. Singal, *Large peculiar motion of the solar system from the dipole anisotropy in sky brightness due to distant radio sources*, *The Astrophysical Journal* **742** (2011) L23.
- [12] J. Colin, R. Mohayaee, S. Sarkar and A. Shafieloo, *Probing the anisotropic local universe and beyond with sne ia data*, *Monthly Notices of the Royal Astronomical Society* **414** (2011) 264.
- [13] C. Gibelyou and D. Hutnerer, *Dipoles in the sky*, *Monthly Notices of the Royal Astronomical Society* **427** (2012) 1994.
- [14] M. Rubart and D. J. Schwarz, *Cosmic radio dipole from nvss and wenss*, *Astronomy & Astrophysics* **555** (2013) A117.
- [15] S. Nadathur, *Seeing patterns in noise: gigaparsec-scale ‘structures’ that do not violate homogeneity*, *Monthly Notices of the Royal Astronomical Society* **434** (2013) 398.
- [16] P. Tiwari and P. Jain, *Dipole anisotropy in integrated linearly polarized flux density in nvss data*, *Monthly Notices of the Royal Astronomical Society* **447** (2015) 2658.
- [17] B. Javanmardi, C. Porciani, P. Kroupa and J. Pflamm-Altenburg, *Probing the isotropy of cosmic acceleration traced by type ia supernovae*, *The Astrophysical Journal* **810** (2015) 47.
- [18] S. Appleby, A. Shafieloo and A. Johnson, *Probing bulk flow with nearby sne ia data*, *The Astrophysical Journal* **801** (2015) 76.
- [19] H.-N. Lin, S. Wang, Z. Chang and X. Li, *Testing the isotropy of the universe by using the jla compilation of type ia supernovae*, *Monthly Notices of the Royal Astronomical Society* **456** (2016) 1881.
- [20] J. Colin, R. Mohayaee, M. Rameez and S. Sarkar, *High-redshift radio galaxies and divergence from the cmb dipole*, *Monthly Notices of the Royal Astronomical Society* **471** (2017) 1045.
- [21] P. Tiwari and P. K. Aluri, *Large angular-scale multipoles at redshift 0.8*, *The Astrophysical*

*Journal* **878** (2019) 32.

- [22] P. Tiwari and P. Jain, *Evidence of isotropy on large distance scales from polarizations of radio sources*, *Astronomy & Astrophysics* **622** (2019) A113.
- [23] J. Řípa and A. Shafieloo, *Update on testing the isotropy of the properties of gamma-ray bursts*, *Monthly Notices of the Royal Astronomical Society* **486** (2019) 3027.
- [24] C. A. P. Bengaly, J. S. Alcaniz and C. Pigozzo, *Testing the isotropy of cosmic acceleration with the pantheon+ and sh0es datasets: A cosmographic analysis*, *Physical Review D* **109** (2024) 123533.
- [25] R. Kothari, M. Panwar, G. Singh, P. Tiwari and P. Jain, *A study of dipolar signal in distant quasars with various observables*, *The European Physical Journal C* **84** (2024) 75.
- [26] A. Abghari, E. F. Bunn, L. T. Hergt, B. Li, D. Scott, R. M. Sullivan et al., *Reassessment of the dipole in the distribution of quasars on the sky*, *Journal of Cosmology and Astroparticle Physics* **2024** (2024) 067.
- [27] R. Watkins, T. Allen, C. J. Bradford, A. Ramon, A. Walker, H. A. Feldman et al., *Analysing the large-scale bulk flow using cosmicflows4: increasing tension with the standard cosmological model*, *Mon. Not. Roy. Astron. Soc.* **524** (2023) 1885 [2302.02028].
- [28] A. M. Whitford, C. Howlett and T. M. Davis, *Evaluating bulk flow estimators for CosmicFlows-4 measurements*, *Mon. Not. Roy. Astron. Soc.* **526** (2023) 3051 [2306.11269].
- [29] PLANCK collaboration, *Planck 2018 results. I. Overview and the cosmological legacy of Planck*, *Astron. Astrophys.* **641** (2020) A1 [1807.06205].
- [30] PLANCK collaboration, *Planck 2013 results. XXVII. Doppler boosting of the CMB: Eppure si muove*, *Astron. Astrophys.* **571** (2014) A27 [1303.5087].
- [31] F. Marocco, P. R. M. Eisenhardt, J. W. Fowler, J. D. Kirkpatrick, A. M. Meisner, E. F. Schlafly et al., *The catwise2020 catalog*, *The Astrophysical Journal Supplement Series* **253** (2021) 8.
- [32] J. J. Condon, W. D. Cotton, E. W. Greisen, Q. F. Yin, R. A. Perley, G. B. Taylor et al., *The nrao vla sky survey*, *The Astronomical Journal* **115** (1998) 1693.
- [33] N. J. Secrest, S. von Hausegger, M. Rameez, R. Mohayaee and S. Sarkar, *A Challenge to the Standard Cosmological Model*, *Astrophys. J. Lett.* **937** (2022) L31 [2206.05624].
- [34] A. K. Singal, *Large disparity in cosmic reference frames determined from the sky distributions of radio sources and the microwave background radiation*, *Phys. Rev. D* **100** (2019) .
- [35] T. M. Siewert, M. Schmidt-Rubart and D. J. Schwarz, *Cosmic radio dipole: Estimators and frequency dependence*, *Astron. Astrophys.* **653** (2021) A9.
- [36] O. T. Oayda, V. Mittal, G. F. Lewis and T. Murphy, *A bayesian approach to the cosmic dipole in radio galaxy surveys: joint analysis of nvss rcs*, *Mon. Not. Roy. Astron. Soc.* **531** (2024) 4545.
- [37] F. Crawford, *Detecting the cosmic dipole anisotropy in large-scale radio surveys*, *Astrophys. J.* **692** (2009) 887.
- [38] M. Rubart, D. Bacon and D. J. Schwarz, *Impact of local structure on the cosmic radio dipole*, *Astron. Astrophys.* **565** (2014) A111.
- [39] P. Tiwari and A. Nusser, *Revisiting the nvss number count dipole*, *JCAP* **03** (2016) .
- [40] J. Darling, *The universe is brighter in the direction of our motion: Galaxy counts and fluxes are consistent with the cmb dipole*, *Astrophys. J. Lett.* **931** (2022) L14.
- [41] J. D. Wagnveld, H.-R. Klöckner and D. J. Schwarz, *The cosmic radio dipole: Bayesian estimators on new and old radio surveys*, *Astron. Astrophys.* **675** (2023) A72.

- [42] V. Mittal, O. T. Oayda and G. F. Lewis, *The Cosmic Dipole in the Quiaia Sample of Quasars: A Bayesian Analysis*, *Mon. Not. Roy. Astron. Soc.* **527** (2024) 8497 [[2311.14938](#)].
- [43] L. Dam, G. F. Lewis and B. J. Brewer, *Testing the cosmological principle with catwise quasars: a bayesian analysis of the number-count dipole*, *Monthly Notices of the Royal Astronomical Society* **525** (2023) 231.
- [44] O. T. Oayda, V. Mittal, G. F. Lewis and T. Murphy, *A Bayesian approach to the cosmic dipole in radio galaxy surveys: joint analysis of NVSS & RACS*, *Mon. Not. Roy. Astron. Soc.* **531** (2024) 4545 [[2406.01871](#)].
- [45] EBOSS collaboration, *The SDSS-IV extended Baryon Oscillation Spectroscopic Survey: Overview and Early Data*, *Astron. J.* **151** (2016) 44 [[1508.04473](#)].
- [46] K. M. Górski, E. Hivon, A. J. Banday, B. D. Wandelt, F. K. Hansen, M. Reinecke et al., *HEALPix - A Framework for high resolution discretization, and fast analysis of data distributed on the sphere*, *Astrophys. J.* **622** (2005) 759 [[astro-ph/0409513](#)].
- [47] G. F. R. Ellis and J. E. Baldwin, *On the expected anisotropy of radio source counts*, *Monthly Notices of the Royal Astronomical Society* **206** (1984) 377.
- [48] S. D. Landy and A. S. Szalay, *Bias and variance of angular correlation functions*, *The Astrophysical Journal* **412** (1993) 64.
- [49] P. Tiwari, G.-B. Zhao and A. Nusser, *The Clustering Properties of AGNs/Quasars in CatWISE2020 Catalog*, *Astrophys. J.* **943** (2023) 116 [[2207.09477](#)].